Contents lists available at: http://qu.edu.iq

Al-Qadisiyah Journal for Engineering Sciences

Journal homepage: https://qjes.qu.edu.iq

Research Paper

Circulating power analysis in dual-input planetary gear mechanisms employed in in-wheel motor-driven electrical vehicles

Gaidaa Shaker Kareem* and *Essam L. Esmail

Department of Mechanical Engineering, College of Engineering, University of Al-Qadisiyah, Diwaniyah, 58001, Iraq.

ARTICLE INFO

Article history:
Received 30 January 2024
Received in revised form 11 April 2024
Accepted 04 April 2025

keyword:
Nomogragh
Two input
Gear ratio
Velocity ratio
Power flow
Power losses
Electric vehicles

ABSTRACT

Electric vehicles (EVs) are known for their power efficiency and lower pollution levels compared to traditional vehicles. The design of dual-motor EV systems, utilizing planetary gear trains, is a significant area of research. The impact of power circulation on losses in novel and patented planetary gear mechanisms has not been extensively explored in previous configuration design studies, despite its importance as a key component of the mechanism. Accurately understanding the power distribution in a dual-motor system seems to be crucial for fully comprehending an invention. This paper explores the positive aspects and drawbacks of PGT configuration, with a focus on efficiency, which may affect competitiveness in real-world applications. If power flow estimation is not possible or if operating constraints prevent it, it is likely that the patent was not thoroughly examined or the inventor lacked experience in the subject matter. A nomograph is a graphical tool used to analyze the relationships between variables in power-split systems, including power flow and efficiency. A systematic approach is proposed for evaluating the performance and power loss of PGTs. Analytical formulas for powers, losses, and efficiency are derived. A parametric study on a wheel hub motor reveals that a higher gear ratio enhances efficiency and performance, with power flow analysis indicating power circulation and amplification. Controlling gear ratios precisely can change power flow direction, enhancing efficiency. Criteria for no power circulation are established, leading to a new configuration.

1. Introduction

Environmental issues have received a lot of attention globally in recent decades, which has increased consumer interest in eco-friendly automobiles. When compared to other traditional cars, electric vehicles (EVs) use less energy and produce less pollution. [1, 2]. This interest has extended across various industries, including the automotive, commercial, agriculture, and construction sectors, all of which have actively contributed to eco-friendly vehicles development. Extensive research has been conducted in multiple areas to advance the field of eco-friendly vehicles [3–6]. The EVs design of system configuration is one of the most explored study issues for energy efficiency and improvement performance of the vehicle in dual-motor systems of EV [7–10]. In recent years, many studies have been conducted on the topics of performance optimization and system configuration for energy efficiency, such as the design of two-engine systems with planetary gear trains for electric tractors [11–14] and a novel dual-motor EV transmission by synchronizers for heavy-duty vehicles [15]. Even when these dual - motor systems based on planetary gear trains offer certain advantages in terms of energy efficiency, they have significant disadvantages that can add losses due to splitting the input power which results in the power circulation in the system. Daisuke and Gunji et al. [16] proposed the wheel hub motor in 2014, which has two distinct motors and a transmission comprised of two planetary gear trains capable of delivering both high drive torque and high speeds (see Fig. 1). Where 11 - First motor, 12 - Second motor, 20 - First planetary gear mechanism, 21 - First sun gear, 23 - First carrier, 24 - First ring gear, 30 - Second planetary gear mechanism, 31 - Second sun gear, 33 - Second carrier, 34 - Second ring gear, 40 - Clutch device, 49 - Clutch output shaft, 50 Wheel bearing, G - Gear ratio, T1(TA), T3 - Output torques under different operating conditions of clutch 40.

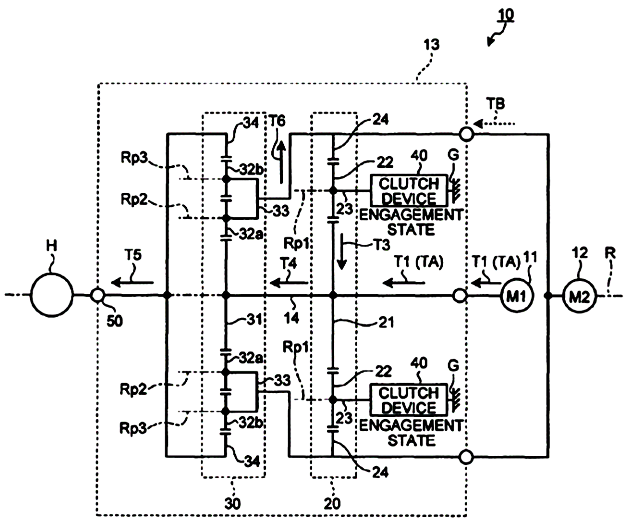

Figure 1. A wheel hub motor for driving an electric vehicle [16].

*Corresponding Author.
E-mail address: essam.esmai@qu.edu.iq ; Tel: (+964) 780-4344 2187 (Essam Esmail)

https://doi.org/10.30772/qjes.2024.146323.1102

Nomenclature

ω	Angular velocity (rad/s)	T	Torque (Nm)
η	Efficiency	R	Gear ratio
p	Power ($watt$)	β	Input angular velocity ratio
l	Power losses ($watt$)	PGE	Planetary gear entity
z	Teeth number of gear	eco	Economy

The transmission mechanism allows smooth gear-change even during acceleration by managing the torque and speed of the two motors. During high-gear operation, the two motors revolve in the same direction. When low gearing is required, they revolve in opposing directions. Following that, in 2017, NSK used this patent to improve on the actual vehicle [17]. It is presently attempting to market certain components such as the wheel hub bearing with integrated speed reducer, one way clutch, and wheel hub motor [18]. Yang et al. [19] proposed a method to find the optimal configurations with high-speed ratio to satisfy the high-power density in-wheel motor.

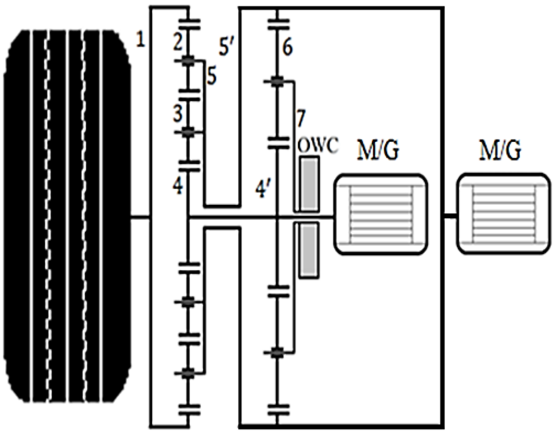

Figure 2. A schematic drawing of the compound power split mechanism integrated into IWM [17].

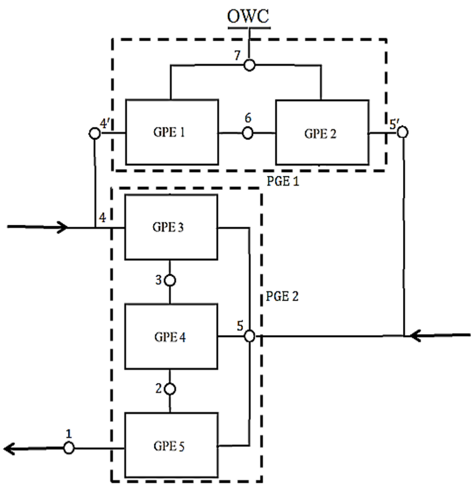

Figure 3. The simplified representation of mechanism depicted in Fig. 2.

Power circulation is a common phenomenon in planetary gear trains, where power flows differently through the various elements of the system compared to the power being transmitted. When power flows through closed paths in planetary gear trains, there can be instances of power circulation. This means that some of the input power ends up circulating within the mechanical systems instead of being delivered to the desired output. This phenomenon, influenced by the gear members relative motion, significantly impacts the efficiency and performance of systems that transmitting power continuously. Power re-circulating can be small or significant, depending on the planetary gear system's kinematic structure. Failure in such systems can occur if the concept of circulating power is not recognized. To minimize re-circulating power size and increase efficiency, the design of transmissions with planetary gear trains considers power circulation, because it does not produce any useful output work. A key step in evaluating new concepts and patents that use planetary gear mechanisms is to examine their configuration and how it affects power circulation and system efficiency. Because the configuration indicates the "coreöf the mechanism, it may cause power circulation, resulting in more losses. The study investigates the positive aspects and drawbacks of one configuration, emphasizing its impact on efficiency, which may affect its competitiveness in real-world applications. Correctly determining the power flow within a two-motor system appears to be the key to gaining a thorough grasp of an invention. If power flow cannot be determined or if operating constraints preclude it, it is likely that the patent was not thoroughly examined or that the inventor was unfamiliar with the subject. Unfortunately, this issue is not taken into account in any of the past configuration design studies. As a result, an effective method for detecting power circulation in the integrated transmission of the wheel hub motor, as well as an evaluation of the amount of circulating power and its effect on power losses and system efficiency, is required. The present study employs a parametric approach to evaluate the impact of design parameters such as the number of gear teeth, local efficiencies, and input velocity ratio on independent variables such as total efficiency, power losses, and power circulation. Also this work attempts to shed light on how to make multipath power flow systems more efficient. This is the first objective of the paper. It is possible to look for conditions where there is reduced or no power circulation and use new or modified configurations to do so. This is accomplished through Objective 2, and the configuration analysis is used to discover the cause of power re-circulation and how to reduce or avoid it.

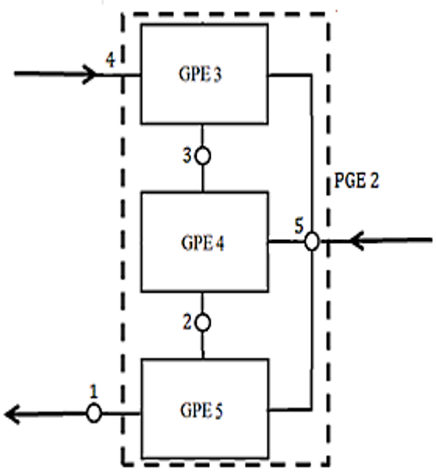

Figure 4. The active double-planet split-power subsystem.

In a compound power-split mechanism, the powertrain typically consists of a planetary gear unit which has a wide range of applications across diverse industrial sectors [20–29], two electric motors, and a generator. The planetary gear unit enables power splitting and combining between the electric motors and the generator. This type of mechanism has been created in practice, but it has not gotten the same level of attention in theoretical investigations. For this reason, the present investigation was undertaken to address a gap in the literature. The general importance of the study stems from the fact that it contributes to establishing a theoretical basis for NSK system, allowing for a better understanding of how power circulation influences system efficiency. Figure 2 shows a schematic drawing of the compound power split mechanism integrated into in wheel motor (IWM) [17]. Figure 3 depicts the schematic representation of the system depicted in Fig. 2. Power is transmitted from one gear per entity (GPE) or planetary gear entity (PGE) to another via common links. PGE 1 is formed from GPE 1 and GPE 2, while PGE 2 is formed from GPE 3, GPE 4, and GPE 5. Before proceeding, we should determine which links are active when the one-way clutch (OWC) is inactive. Power transmits at any link to nearby links (common links) or the environment is considered an active link (fixed, input, and output links). The common links made by links $4(4')$ and $5(5')$ are utilized to deconstruct the mechanism depicted in Fig. 3 into its constituent PGEs: PGE 1 containing links $4'$, $5'$, 6, and 7 and PGE 2 containing links 1, 2, 3, 4, and 5. For differentiation, link 4(5) and link $4'(5')$ are alternative designations for the same common link. When the OWC is inactive, links 1, 4, and 5 become active, resulting in the system being reduced to a single PGE as shown in Fig. 4.

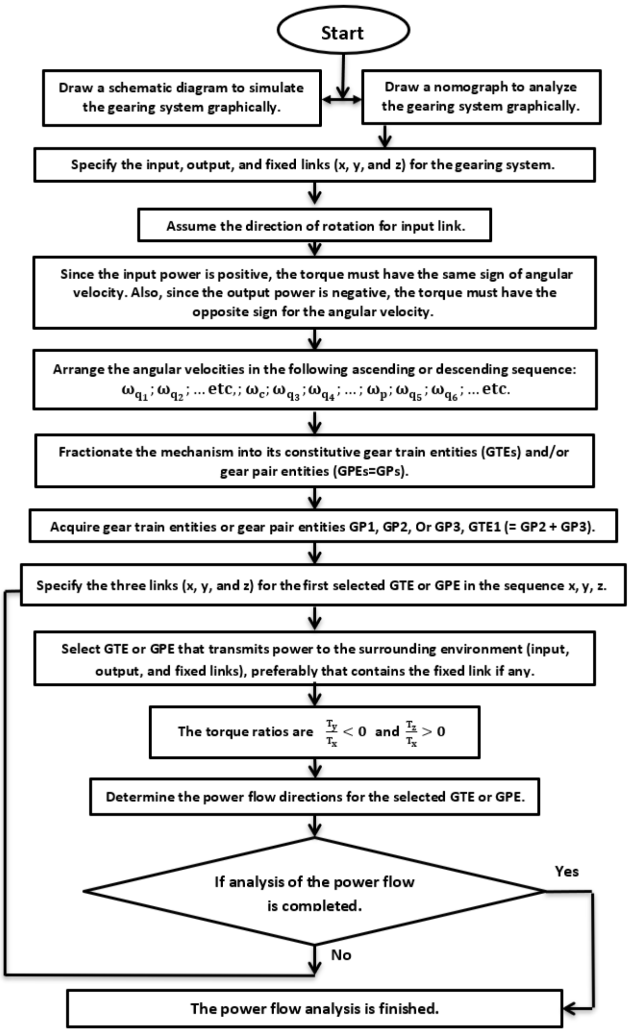

Figure 5. The major steps of the power flow analysis methodology.

The following flow chart, Fig. 5 shows the major steps of the power flow analysis methodology. The paper is organized as following: Section 1 of the paper introduces the background and context of the study, emphasizing the worldwide interest in eco-friendly vehicles and the necessity for appropriate system configurations. The compound power-split mechanism is an alternate arrangement for electric vehicle drive systems. The Nomograph is introduced in Section 2 as a graphical computation tool for determining complex relationships between variables. Section 3 explains how to use a nomograph to detect the power circulation through the elements of a compound power-split mechanism. In section 4, a systematic approach for studying and calculating the efficiency and power loss of PGT is proposed. Analytical expressions are derived for the powers, power losses, and efficiency. Following that in Section 5, the results of the preceding section has been verified. In section 6, the total efficiency is calculated using the friction losses. The planetary gear configuration used in the wheel hub motor is examined. In most cases, the system's overall efficiency is enhanced by precisely regulating the gear ratios, which in turn adjust the power flow within the system. The conditions for no power circulation are determined, and an alternative configuration is proposed in section 7. Also in section 8, limitations to find total efficiency in PGT. And finally, in section 9, certain conclusions are derived.

2. Nomograph

A nomograph is a graphical calculation tool that allows for the quick determination of complex relationships between different variables. In the case of the compound power-split mechanism, a nomograph could be constructed to represent the efficiency as a function of various parameters, such as velocity ratio, and operating conditions. The "velocity ratio"$R^{v}_{(w,u)}$ between links (w and 4) in relation to link (v) of a PGT is expressed as in Eq. 1.

$$R^{v}_{w,u} = \frac{R^{c}_{w,p} - R^{c}_{v,p}}{R^{c}_{u,p} - R^{c}_{v,p}} = \frac{\omega_w - \omega_v}{\omega_u - \omega_v} \tag{1}$$

Where links w, u, and v are from distinct GPEs, while links p and c are common. The gear q, planet gear p, as well as the planet-gear-carrier c, distinguish the GPE. PGTs are constructed from GPEs. Figure 2 shows how the GPE is depicted for power flow analysis.

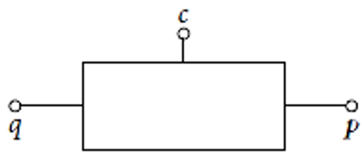

Figure 6. Schematic representation of a GPE.

Equation 1 can be used to get the planet gear ratio $R^{c}_{q,p}$ for a GPE as shown in Eq. 2.

$$R^{v}_{q,p} = \frac{R^{c}_{q,p} - R^{c}_{c,p}}{R^{c}_{p,p} - R^{c}_{c,p}} = \frac{\omega_q - \omega_c}{\omega_p - \omega_c} \tag{2}$$

Where $R^{c}_{p,p} = 1$ and $R^{c}_{c,p} = 0$. In relation to the number of teeth Z_p and Z_q, $R^{c}_{q,p}$ can alternatively be expressed as in Eq. 3.

$$R^{v}_{q,p} = \pm \frac{Z_p}{Z_q} \tag{3}$$

Internal gears are denoted by a plus sign, whereas external gears are denoted by a minus sign. The "planet gear ratio"for any GPE is represented by the Eq. 4, Eq. 5, and Eq. 6 respectively.

$$R^{5}_{1,2} = \frac{Z_2}{Z_1} \tag{4}$$

$$R^{5}_{3,2} = \frac{\omega_3 - \omega_c}{\omega_2 - \omega_c} = -\frac{Z_2}{Z_3} \tag{5}$$

$$R^{5}_{4,3} = \frac{\omega_4 - \omega_c}{\omega_3 - \omega_c} = -\frac{Z_3}{Z_4} \tag{6}$$

By multiplying $R^{5}_{3,2}$ by $R^{5}_{4,3}$, we get, Eq. 7.

$$R^{5}_{3,2} R^{5}_{4,3} = \frac{\omega_3 - \omega_c}{\omega_2 - \omega_c}\frac{\omega_4 - \omega_c}{\omega_3 - \omega_c} = \frac{\omega_4 - \omega_c}{\omega_2 - \omega_c} = R^{5}_{4,2} = \frac{Z_2}{Z_4} \tag{7}$$

The ring gear 1 is always larger than the sun gear 4, $Z_1 > Z_4$, hence $1/Z_1 < 1/Z_4$, therefore $Z_2/Z_1 < Z_2/Z_4$ or $R^{5}_{1,2} < R^{5}_{4,2}$. Since the range of $R^{5}_{4,2}$ is identified as $R^{5}_{4,2} > R^{5}_{1,2}$, three possible subcases exist:

1) $If\ \frac{Z_2}{Z_4} < 1\ or\ Z_2 < Z_4,\ then\ 1 > R^{5}_{4,2} > R^{5}_{1,2}$

2) $If\ \frac{Z_2}{Z_4} = 1\ or\ Z_2 = Z_4,\ then\ 1 = R^{5}_{4,2} > R^{5}_{1,2}$

3) $If\ \frac{Z_2}{Z_4} > 1\ or\ Z_2 > Z_4,\ then\ R^{5}_{4,2} > 1 > R^{5}_{1,2}$

Here we looked at the first case. The characteristic parameter Z_1/Z_4 of the PGT should be regarded as a variable ranging from 1.2 to 4. The "planet gear ratiosöften determine how the nomograph is drawn. The nomograph of the PGT illustrated in Fig. 7 is displayed in Fig. 8 and Fig. 9 for two cases.
The case 1, shown if Fig. 8, we have $\omega_2 > \omega_4 > \omega_1 > \omega_5 > \omega_3 > 0$.
In case 2, shown if Fig. 9, we have $\omega_3 > \omega_5 > \omega_1 > \omega_4 > \omega_2 > 0$.

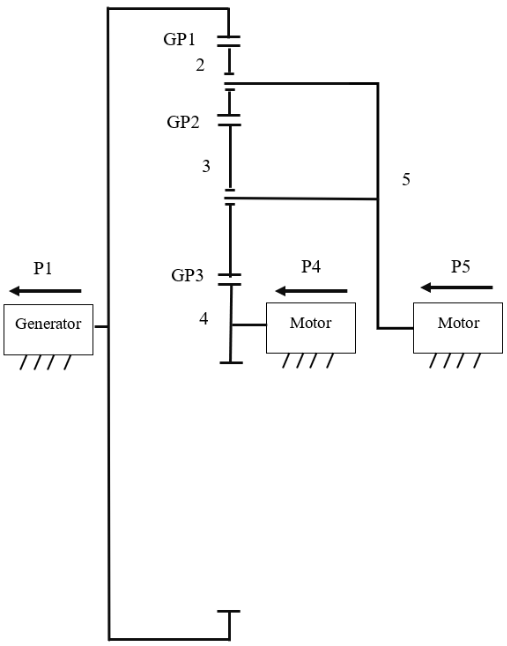

Figure 7. A typical PGT with three GPEs.

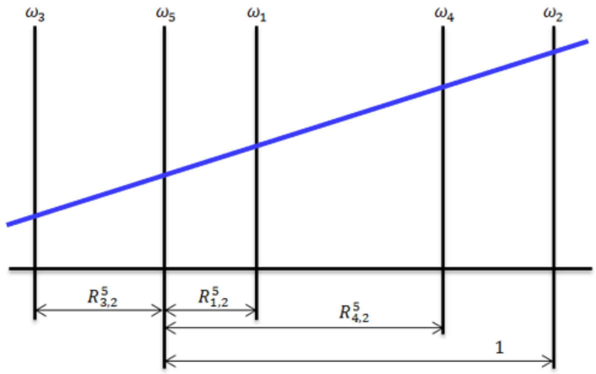

Figure 8. The nomograph of the PGT shown in Fig. 7 when $(\omega_2 > \omega_4 > \omega_1 > \omega_5 > \omega_3 > 0)$

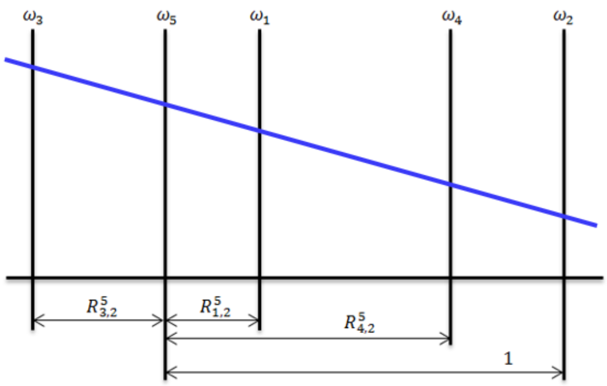

Figure 9. The nomograph of the PGT shown in Fig. 7 when $(\omega_3 > \omega_5 > \omega_1 > \omega_4 > \omega_2 > 0)$.

3. Power flow through the mechanism

Let us consider the case when links 4 and 5 are inputs (see Fig. 10). In accordance with the nomograph approach [30], the torque vector directing upward is positive, whereas the torque vector pointing downward is negative. In addition, the velocity also has a positive value above and a negative value below the line of zeros. Hence, the input power is the product of positive torque at positive velocity or negative torque at negative velocity. Suppose that sun gear 4 turns positively counter clockwise. Because sun gear 4 is an input link $(T_4\ \omega_4 > 0)$ and $\omega_4 > 0$, $T_4 > 0$ must be an upward vector. As a result, the torque vector of the ring gear 1 point downward $(T_1 < 0\ )$ and the carrier 5 must point upward $(T_5 > 0)$. Because carrier 5 is an input link $(T_5\ \omega_5 > 0)$ and $T_5 > 0$, so $\omega_5 > 0$. Also, since ring gear 1 is an output link $(T_1\ \omega_1 < 0)$ and $T_1 < 0$, therefore $\omega_1 > 0$. Figure 10 is the monograph created for this gear train for case 1, with the torque vectors drawn according to the nomograph methodology. Similarly case 2 given in Fig. 9 can be drawn (not shown).

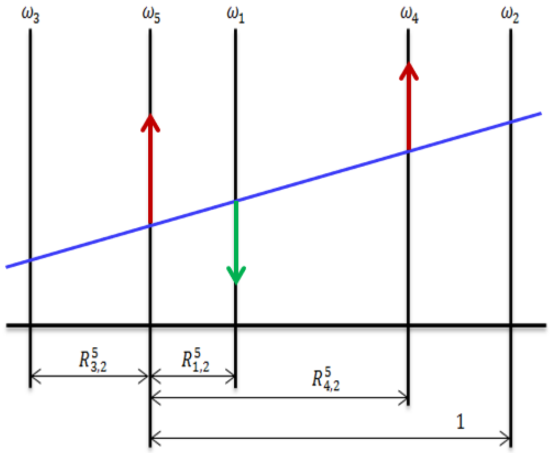

Figure 10. The double-planet PGE having links 4 and 5 as inputs.

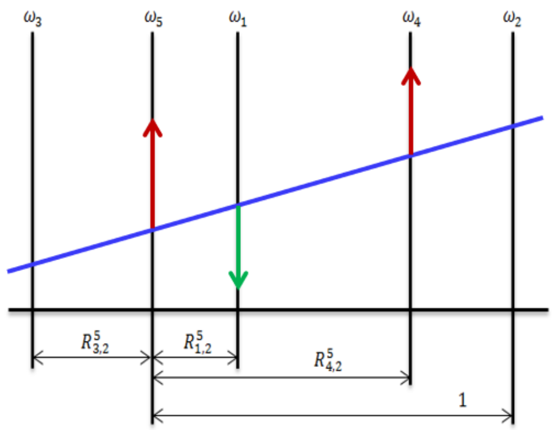

Figure 11. The power equilibrium of the PGT depicted in Fig. 10.

Because power might travel through multiple paths in the mechanism, there is a chance that some of it may loop back inside the mechanism rather than reaching the output link. As a result, we must investigate the power flow across the constituents of the system. This can be best shown on the GPE diagram shown in Fig. 12.

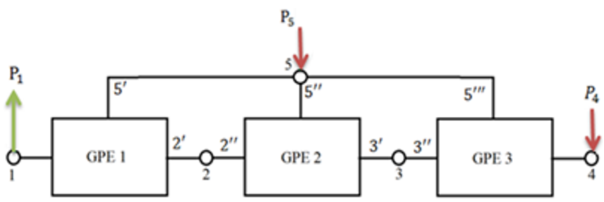

Figure 12. The GPE diagram.

3.1 Flow of power via GPE 1

GPE1 is made up of GP1 and planet carrier 5. Because the ring gear 1 is an output link ($T_1\ \omega_1 < 0$), and $\omega_1 > 0$, T_1 must be a vector pointing downward. This means that the torque vectors of planet gear 2 and carrier 5 must both point upward $T_{2'} > 0$ and $T_{5'} > 0$). Since $\omega_2 > \omega_5 > 0$, therefore $P_{2'} = T_{2'}\ \omega_2 > 0$, and $P_{5'} = T_{5'}\ \omega_5 > 0$. In GPE1, the inputs are links 2 and 5, while the output is link 1. (See Fig. 13).

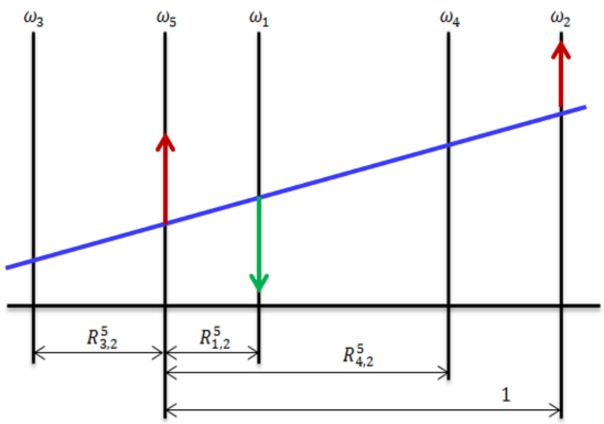

Figure 13. The power equilibrium of GPE1.

Because link 2 ($2'$ and $2''$) is a shared link between GTE 1 and GTE 2, the input power to GTE 1 (P_2') equals the output power from GTE 2 ($P_{2''}$). Because link 2 ($2'$ and $2''$) joins GTE 1 and GTE 2, the input power to GTE 1(P_2') serves as the power output for GTE 2($P_{2''}$). This means that $P_{2'} + P_{2''} = 0$.

3.2 Flow of power via GPE 3

GPE3 is made up of GP3 and planet carrier 5. Because the sun gear 4 is an input link ($T_4\ \omega_4 > 0$) and $\omega_4 > 0$, T_4 must be a vector pointing upward. This implies that the torque vector of planet gear 3 must point upward and the torque vector of carrier 5 must point downward ($T_{3''} > 0$ and $T_{5'''} < 0$.

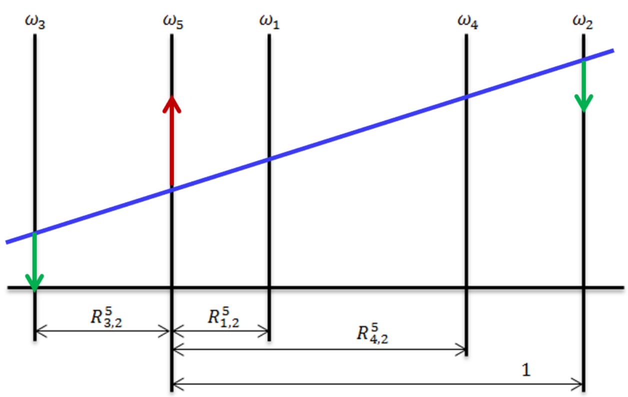

Figure 14. The power equilibrium of GPE3.

Since $\omega_4 > 0$, $\omega_5 > 0$, $\omega_3 > 0$, therefore $P_{3''} = T_{3''}\ \omega_3 > 0$, and $P_{5'''} = T_{5'''}\ \omega_5 < 0$. In GPE3, the input links are 4 and 3, and link 5 is the output link (see Fig. 3). Since link 3 ($3'$ and $3''$) is a common link between GTE 2 and GTE 3, then the input power to GTE 3 ($P_{3''}$) is the output power from GTE 2($P_{3'}$). This means that $P_{3'} + P_{3''} = 0$.

3.3 Flow of power via GPE 2

GPE2 is made up of GP2 and planet carrier 5. Because the planet gear 2 is output link ($T_{2''}$) $\omega_2 < 0$) and $\omega_2 > 0$, $T_{2''}$) must be a vector pointing downward. Furthermore, $T_{3'} < 0$suggests that T_3' is a vector pointing downward because the planet gear 3 is an output link ($T_{3'}\ \omega_3 < 0$ and $\omega_3 > 0$. This implies that the torque vector of planet gear carrier 5 must point upward ($T_{5''} > 0$). Since $\omega_2 >\ \omega_5 >\ \omega_3 > 0$, therefore $P_{5''} = T_{5''}\ \omega_5 > 0$. In contrast to links 2 and 3 in GPE2, which are output links, link 5 is an input link (see Fig. 15).

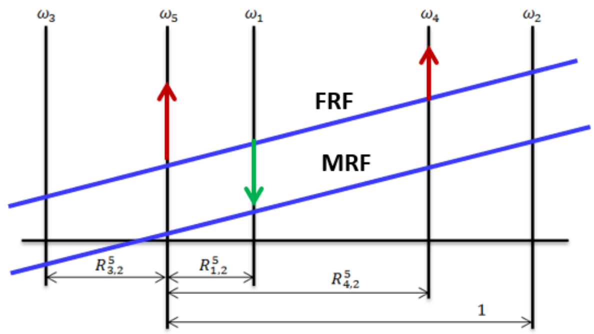

Figure 15. The power equilibrium of GPE2.

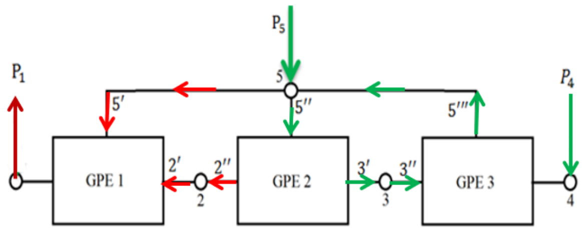

Figure 16. Power circulation in double-planet gear train for both cases.

Based on the results of Fig. 11 through Fig. 15, there is power circulation through links $3'$, $3''$, $5''$ and $5'''$ for both cases. The power circulation can be visualized in Fig. 16.

4. Efficiency formula derivation

When the planet carrier is virtually fixed in the moving reference frame (MRF):

1. Link i will be designated as a driving link and assigned as (x) when $P_i^c > 0$.
2. Link i will be designated as a driven link and assigned the symbol (y) when $P_i^c < 0$.
3. The fixed reference frame (FRF) and MFR are identical if the carrier is stationary.

In accordance with the power equilibrium and angular velocity relationships, the powers flowing across any PGE are interrelated as shown in Eq. 8.

$$\frac{P_x}{R^z_{y,x}} = -\frac{P_y}{\eta_{z(x-y)} R^f_{y,x}} = \frac{P_z}{\left(\eta_{z(x-y)} - R^z_{y,x}\right) R^f_{z,x}} = \frac{P^z_x}{R^z_{y,x} R^x_{z,f}} \tag{8}$$

The friction loss (l) caused by each PGE are calculated as the product of P_x^c and $(\eta_c - 1)$. It can be written as, Eq. 9.

$$l = (\eta_c - 1)\, P_x^c \tag{9}$$

For case 1, Fig. 17 depicts the PGT in the fixed reference frame (FRF) and moving reference frame (MRF). Link 4 is the input link in both frames, and link 1 is the output link.

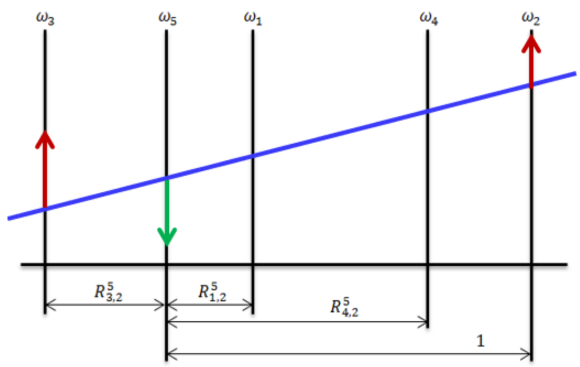

Figure 17. Power equilibrium in the FRF and MRF when ($\omega_2 > \omega_4 > \omega_1 > \omega_5 > \omega_3$).

By putting $x=4, y=1, z=5$ into Eq. 8, we get, Eq. 10.

$$\frac{P_4}{R^5_{1,4}} = -\frac{P_1}{\eta_{5(4-1)}R^f_{1,4}} = \frac{P_5}{\left(\eta_{5(4-1)} - R^5_{1,4}\right)R^f_{5,1}} = \frac{P^5_4}{R^5_{1,4}R^4_{5,f}} \tag{10}$$

The loss can be calculated independently for each GP using Eq. 9, to find Eq. 11.

$$l_1 = (\eta_3 - 1)\, P^5_4 \tag{11}$$

Similarly,Eq. 12 and Eq. 13 were develop.

$$l_2 = \eta_3\,(\eta_2 - 1)\, P^5_4 \tag{12}$$

$$l_3 = \eta_3\eta_2\,(\eta_1 - 1)\, P^5_4 \tag{13}$$

When these three equations are combined and after simplification, the total power loss can be written as Eq. 14.

$$l_t = (\eta_3\eta_2\eta_1 - 1)\, P^5_4 \tag{14}$$

But from Eq. 10, we have:

$$P^5_4 = \frac{R^5_{1,4}R^4_{5,f}}{\eta_{5(4-1)}R^f_{1,4}}P_1 \tag{15}$$

After simplification, we get Eq. 16.

$$P^5_4 = \frac{R^1_{5,f}}{\eta_{5(4-1)}}P_1 \tag{16}$$

The velocity ratio $R^1_{5,f}$ can be written as Eq. 17.

$$R^1_{5,f} = \frac{(\beta - 1)}{\beta R^5_{4,1} - (\beta - 1)} \tag{17}$$

Where the input velocity ratio $= R^f_{5,4} = \omega_5/\omega_4$ and $R^5_{4,1} = Z_1/Z_4$. Substituting Eqs. 15, 16, and 17 into Eq. 14, yields the following simplified formula for l_t in terms of P_1, Eq. 18.

$$l_t = \frac{(\eta_3\ \eta_2\ \eta_1 - 1)(\beta - 1)}{\eta_3\ \eta_2\ \eta_1\ \left(\beta R^5_{4,1} - \beta + 1\right)}P_1 \tag{18}$$

To find the total efficiency of the PGT, substitute Eq. 18 into $_p = 1/(1 + l/P_{out})$, where $P_{out} = P_1$, to obtain after simplification, Eq. 19.

$$\eta_c = \frac{\eta_3\ \eta_2\ \eta_1 - 1\left(\beta R^5_{4,1} - \beta + 1\right)}{\eta_3\ \eta_2\ \eta_1\ \beta R^5_{4,1} - \beta + 1} \tag{19}$$

Also $\eta_{5,1-4} = -P_{out}/P_{in}$, $P_{out} = P_1$ [Let $P_{in} = 1$ so $P_1 = -\eta_c$] to get Eq. 20.

$$P_1 = -\frac{\eta_3\ \eta_2\ \eta_1\left(\beta R^5_{4,1} - \beta + 1\right)}{\eta_3\ \eta_2\ \eta_1\ \beta R^5_{4,1} - \beta + 1} \tag{20}$$

By substitute Eq. 18 in to Eq. 20, will get Eq. 21.

$$l_t = -\frac{(\eta_3\ \eta_2\ \eta_1 - 1)\,(\beta - 1)}{\eta_3\ \eta_2\ \eta_1\ \beta R^5_{4,1} - \beta + 1} \tag{21}$$

From Eq. 16 and Eq. 20, we can get Eq. 22.

$$P^5_4 = -\frac{(\beta - 1)}{\eta_3\ \eta_2\ \eta_1\ \beta R^5_{4,1} - \beta + 1} \tag{22}$$

From Eq. 10 and Eq. 22, we get Eq. 23 and Eq. 24.

$$P_4 = \frac{1}{\eta_3\ \eta_2\ \eta_1\ \beta R^5_{4,1} - \beta + 1} \tag{23}$$

$$P_5 = \frac{\eta_3\ \eta_2\ \eta_1\ \beta R^5_{4,1} - \beta}{\eta_3\ \eta_2\ \eta_1\ \beta R^5_{4,1} - \beta + 1} \tag{24}$$

The input power ratio is expressed as Eq. 25.

$$\frac{P_5}{P_4} = \eta_3\ \eta_2\ \eta_1\ \beta R^5_{4,1} - \beta \tag{25}$$

Now for case 2 and by using a similar procedure to case 1, Fig. 18 depicts the PGT in the FRF and MRF. Link 1 is the input link in the MRF, and link 4 is the output link. By putting $x=1, y=4, z=5$ into Eq. 8, we find that, Eqs. 26 up tp Eq. 32.

$$l_t = (\eta_3\ \eta_2\ \eta_1 - 1)P^5_1 \tag{26}$$

$$\eta_c = \frac{\left(\beta R^5_{4,1} - \beta + 1\right)}{\beta R^5_{4,1} + \eta_3\ \eta_2\ \eta_1(\beta - 1)} \tag{27}$$

$$P_1 = -\frac{\left(\beta R^5_{4,1} - \beta + 1\right)}{\beta R^5_{4,1} + \eta_3\ \eta_2\ \eta_1(\beta - 1)} \tag{28}$$

$$P^5_1 = -\frac{(\beta - 1)}{\eta_3\ \eta_2\ \eta_1\beta R^5_{4,1} - \beta + 1)} \tag{29}$$

$$l_t = -\frac{(\eta_3\ \eta_2\ \eta_1 - 1)\,(\beta - 1)}{\eta_3\ \eta_2\ \eta_1\beta R^5_{4,1} - \beta + 1} \tag{30}$$

$$P_4 = \frac{\eta_3\ \eta_2\ \eta_1}{\beta R^5_{4,1} + \eta_3\ \eta_2\ \eta_1(1 - \beta)} \tag{31}$$

$$P_5 = 1 - P_4$$

$$P_5 = \frac{\beta(R^5_{1,4} - \eta_3\ \eta_2\ \eta_1)}{\beta R^5_{4,1} + \eta_3\ \eta_2\ \eta_1(1 - \beta)} \tag{32}$$

The input power ratio is expressed as Eqs. 33.

$$\frac{P_5}{P_4} = \frac{\beta(R^5_{1,4} - \eta_3\ \eta_2\ \eta_1)}{\eta_3\ \eta_2\ \eta_1} \tag{33}$$

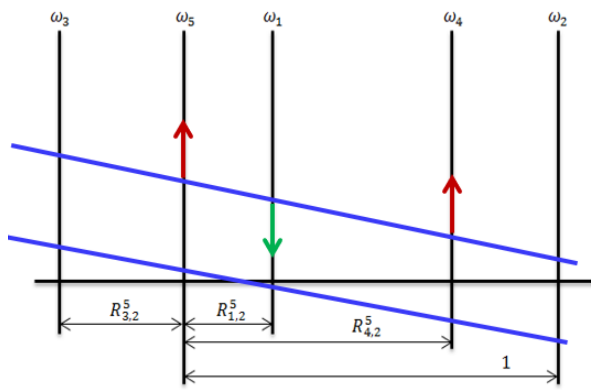

Figure 18. Power equilibrium in the FRF and MRF when ($\omega_3 > \omega_5 > \omega_1 > \omega_4 > \omega_2$).

5. Verification of results

The total efficiency is dependent on the efficiencies of the GPs $\eta_1,\ \eta_2,\ \eta_3$, the planetary gear train characteristic parameter Z_1/Z_4, and the input velocity ratio $\beta = \omega_5/\omega_4$.

1. Assume that the efficiencies of GP 1, 2, and 3 as $\eta_1 = \eta_2 = \eta_3 = 1$. Under this condition, and from Eq. 14 and Eq. 26, the losses for both cases are zero, and from Eq. 19, and Eq. 27 the total efficiency is 100%.
2. Let $\eta_1 = \eta_2 = \eta_3 = 0$, under these conditions, the overall losses deteriorate into (-1). As a result, the overall efficiency can only be zero.
3. $\beta = 0 (= \omega_5/\omega_4)$: Because the planet-carrier is fixed, the two-DOF PGT degenerates into a one-DOF system. As a result, the total efficiency must be just $\eta_1\ \eta_2\ \eta_3$.
4. $\beta \to -\infty (= \omega_5/\omega_4)$: Under this condition, the total power loss approaches $(l_t) \to (1-\eta_1\ \eta_2\ \eta_3)/(\eta_1\ \eta_2\ \eta_3\ R^5_{4,1} - 1)$. This indicates that for large values of β, the total power loss l_t approach asymptotically to a specific value. This is due to the fact that the characteristic parameter $Z_1/Z_4 = R^5_{4,1}$ and the coupled efficiency $\eta_1 23 = \eta_1 \times \eta_2 \times \eta_3$, is specific to a particular PGT.
5. We also make the assumption that each of the three GPs has an efficiency of $\eta_1 = \eta_2 = \eta_3 = 0.9$. Depending on Eq. 19, and Eq. 27 the 3D drawing between $\eta_{5,4-1}$, $R^5_{4,1}$, and $\beta = \omega_5/\omega_4$ can therefore be depicted as in Fig. 19.
6. The characteristic parameter Z_1/Z_4 of the PGT should be regarded as a variable from 1.2 to 4. Therefore.

$$1.2 < R^5_{4,1} = \frac{Z_1}{Z_4} < 4$$

The large gear ratio $R^5_{4,1}$ enhances the efficiency of the planetary gear system, despite power circulation, resulting in higher efficiency and lower losses, as shown in Fig. 19 and Fig. 20.

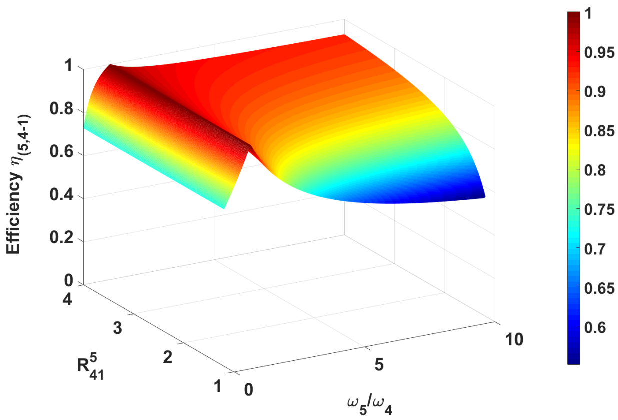

Figure 19**.** The efficiency of the IWM transmission with respect to $R_4, 1^5$ *and* β.

6. Results and discussion

First, the prerequisites for computing the efficiency and power loss formulas must be established.

1. Since $Z_1 > Z_4$, hence, $1 < R^5_{4,1} (= Z_1/Z_4)$.
2. Since the velocity sequence is $\omega_2 > \omega_4 > \omega_1 > \omega_5 > \omega_3 > 0$, then $0 < \beta = \omega_5/\omega_4 < 1$, and since $\omega_3 > \omega_5 > \omega_1 > \omega_4 > \omega_2 > 0$, then $1 < \beta = \omega_5/\omega_4 < \infty$.
3. The individual gear efficiencies are within the physical range of $0 < \eta_i < 1$.

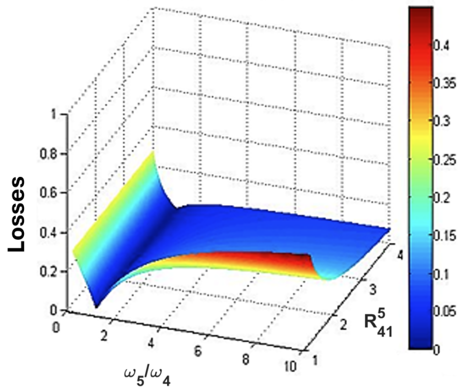

(a) l_t With regard to the input velocity ratio β and the gear ratio $Z_1/Z_(4)$.

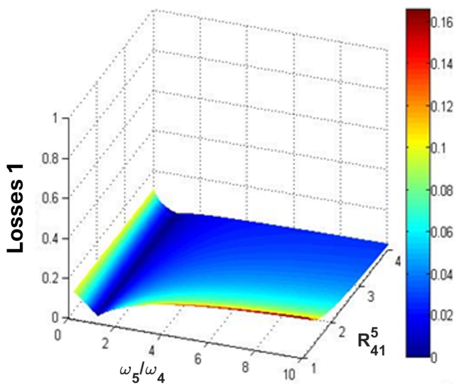

(b) l_1 with regard to the input velocity ratio β and the gear ratio Z_1/Z_4 at gear pair GP3

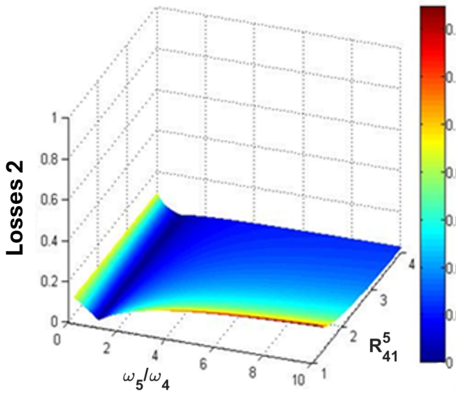

(c) l_2 With regard to the input velocity ratio β and the gear ratio Z_1/Z_4 at gear pair GP2.

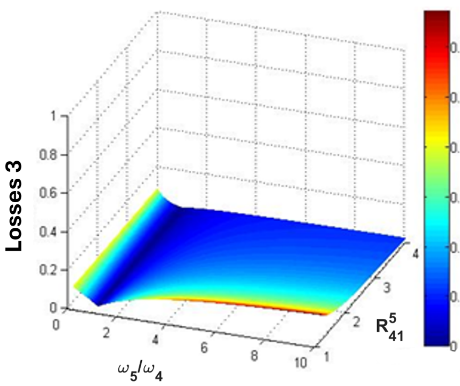

(d) l_3 With regard to the input velocity ratio β and the gear ratio Z_1/Z_4 at gear pair GP1.

Figure 20**.** (a), (b), (c), (d) The power losses at GP1, GP2, GP3 and the total power loss for both cases.

Let the GPs have efficiencies of $\eta_1 = \eta_2 = \eta_3 = 0.9$. Then, using Eq. 21 and Eq. 30, the plot of the cumulative power loss with relation to the input velocity ratio β is shown in Fig. 21 for two gear ratios. When $0 < \beta < 1$, the cumulative power loss l_t start with 0.25 when $\beta = 0$ and approach to zero when $\beta = 1$ for $Z_1/Z_4 = 2.5$ and 3.8, while the cumulative power loss l_t start with 0 at $\beta = 1$ and approaches asymptotically to 0.12 for $Z_1/Z_4 = 2.5$ and 0.08 for $Z_1/Z_4 = 3.8$. In general, the power loss is lower for a higher gear ratio Z_1/Z_4. Figure 22 depicts the power loss for each gear pair as a function of the input velocity ratio β. Figure 23 illustrates that total efficiency exceeds local efficiencies everywhere in its range. Because carrier 5 is an input link, its coupling power is transmitted to links 2 and 3, whereas rolling power is delivered from gear 4 to gears 3, 2, and 1. The power flowing between any interconnected links cannot be greater than the sum of the input power at any endpoint. As a result, the total loss is never greater than the input power, implying that it is less than one. This is because, despite power re-circulation, the coupling power is transmitted directly to the output shaft. Based on Eq. 20, Eq. 23, Eq. 24, Eq. 28, Eq. 31 and Eq. 32, the power balance between the two inputs and the output power are illustrated in Fig. 24. It is apparent that the two input powers are coupled; whenP_5 increases, P_4 must decrease. And when P_5 becomes dominant, losses tend to level off.

7. Condition for reducing the power losses due to power circulation

The large gear ratio $R^5_{4,1}$ enhances the efficiency of the planetary gear system, despite power circulation, resulting in higher efficiency and lower losses, as shown in Fig. 19 and Fig. 20. Assume that the gear ratios are $Z_1/Z_4 = 4$, $Z_3/Z_2 = -1$, and Z_2/Z_4 =1, the local efficiencies are 0.9, and the input velocity ratio β is 0.5. Eq. 20, Eq. 23, and Eq. 24 can be used to determine the output power ($P_1 = -0.930797$) and the two input powers ($P_4 = 0.510725$, and $P_5 = 0.489275$). The negative sign denotes output power. From Eq. 11, Eq. 12, Eq. 13 and Eq. 14, the GPs losses are listed as $l_1 = -0.025536$, $l_2 = -0.022983$, $l_3 = -0.020684$ and $l_t = -0.069203$. Using the powers listed in Table 1. Figure 25 can be drawn to illustrate the power going through the mechanism as well as the losses.

Table 1. Powers flowing through the mechanism.

PGT	GPE1	GPE2	GPE3
P_5=0.8997	$P_5' = 0.8089$	P_5''=0.4028	P_5'''=-0.3119
P_4=0.1003	P_2'=0.1587	P_3'=-0.2228	P_3''=0.2228
P_1=-0.9627	P_1=-0.9627	P_2''=-0.1487	P_4=0.1003
l=-0.0373	l_1=-0.01375	l_2=-0.0124	l_3=-0.0111
P_4+P_5+ $+P_1+l=0$	$P_5'+P_2'+$ $+P_1+l_1=0$	$P_5''+P_3'$ $+P_2''+l_2=0$	$P_5'''+P_3''+$ $+P_4+l_3=0$

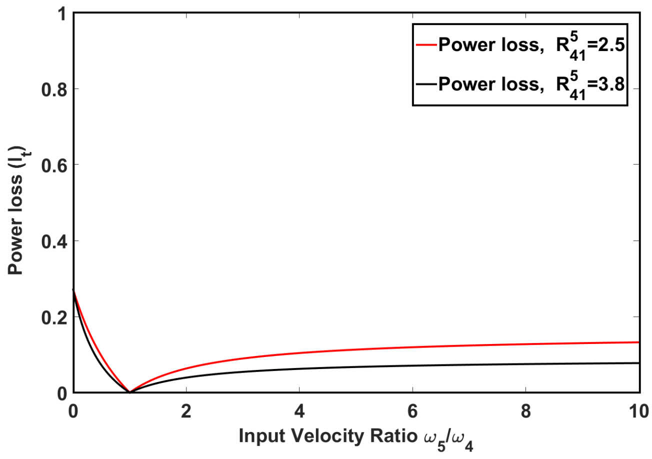

Figure 21**.** The cumulative loss with relation to the input velocity ratio β for the extreme values of $Z_1/Z_4(2.5 and 3.8)$.

Power is amplified as a result of power circulation. The output power of GPE2 ($P_{3'}$) equals the input power of GPE3 with the opposite sign. The power arriving link 5 from GPE3 combines with the power entering link 5 from the motor, amplifying the power. Despite having a little amplified power, the loop in which it circulates experiences increased losses that are proportionate to the amplified power. Figure 25 Power flowing through the PGT. By following the same method as for the first case and the same gear ratios, we find that the powers flowing through the mechanism for case 2 are as in Table 2. The total efficiency in both cases is greater than 93%, which exceeds the assumed local efficiencies of 0.9.

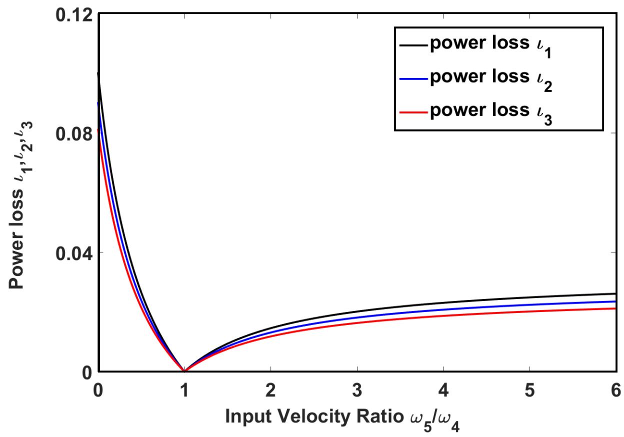

Figure 22**.** The power loss for each gear pair with respect to the input velocity ratio β for the values of $Z_1/Z_4 = 3.8$.

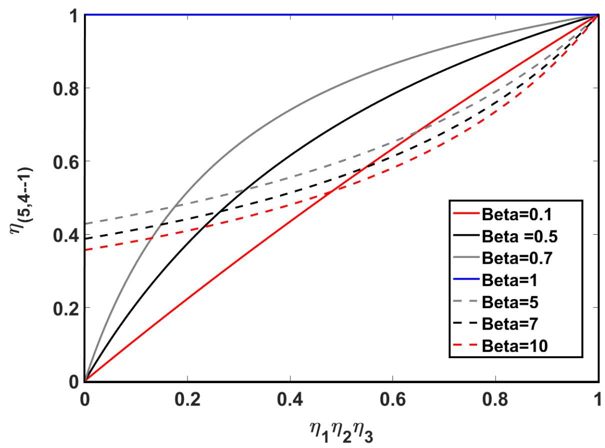

Figure 23**.** Effect of local efficiencies on the total efficiency.

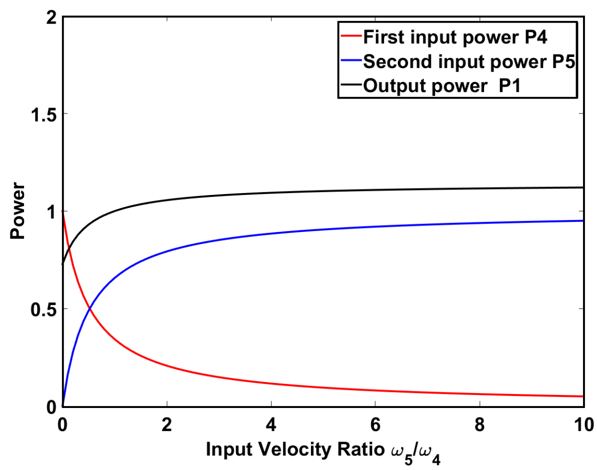

Figure 24**.** The power balance between the two inputs and the output power for both cases.

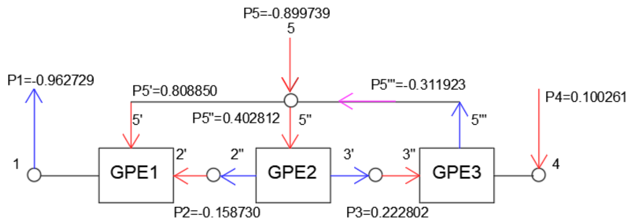

Figure 25. Power flowing through the PGT.

Table 2. Power flowing through the mechanism.

PGT	GPE1	GPE2	GPE3
P_5=0.489275	$P_5' = 0.542645$	P_5''=0.890924	P_5'''=-0.944294
P_4=0.510725	P_2'=0.413688	P_3'=-0.459653	P_3''=0.459653
P_1=-0.930797	P_1=-0.930797	P_2''=-0.413688	P_4=0.510725
l=-0.069203	l_1=-0.025536	l_2=-0.022983	l_3=-0.020684
P_4+P_5+ $+P_1+l=0$	$P_5'+P_2'+$ $+P_1+l_1=0$	$P_5''+P_3'+$ $+P_2''+l_2=0$	$P_5'''+P_3''+$ $+P_4+l_3=0$

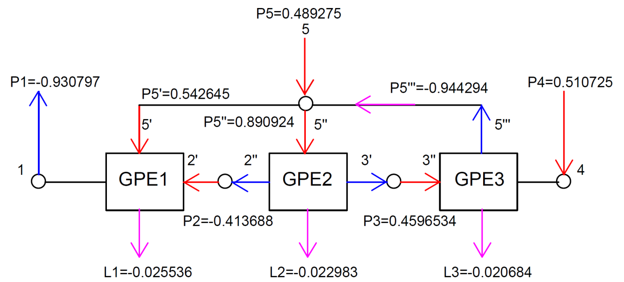

Figure 26. Power flowing through the PGT.

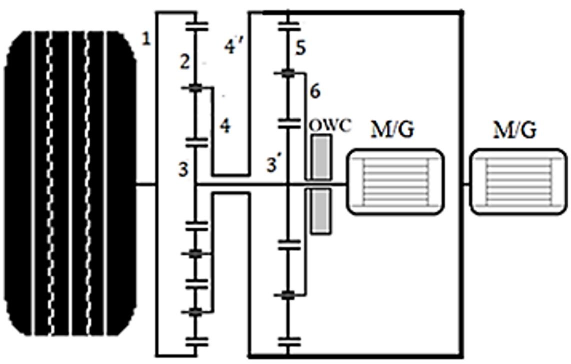

Figure 27. The modified configuration of the PGT of the IWM.

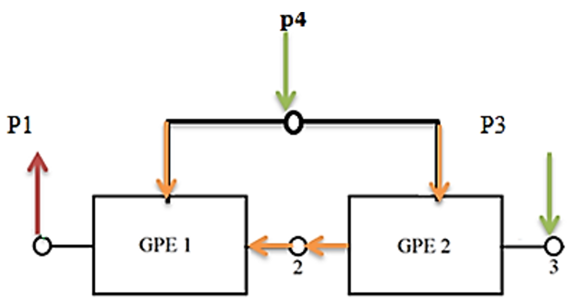

Figure 28. Power flowing through the modified PGT.

7.1 Case for no power circulation

Power circulation occurs when power flows through multiple paths. In the case of a double planet in a compound power-split planetary gear, it can cause power circulation. However, if the system is reduced to a single planet and treated with the same technique, power circulation is less likely to occur. By following the procedure outlined in section 2, the power flow is deduced as shown in Fig. 28. Thus, the most important results of this work can be listed as:

1. By taking advantage of the graph-based method, it is possible to quickly conduct a preliminary power flow analysis that gives a thorough understanding of the power flowing within the system elements.
2. Analysis-based expressions for efficiency and power loss are generated.
3. The power flow analysis indicates that power amplification occurs because of internal power circulation.
4. Power circulation is thoroughly examined. Power circulation is unavoidable in PGTs with multi- planets.
5. he findings are supported by examples.

8. Limitation to find the total efficiency of the PGT

Limitations on estimating the overall efficiency of the planetary gear train (PGT) for electric vehicle in-wheel motor drives include:

1. The three gear pairs (GP1, GP2, and GP3) in the PGT are assumed to have constant efficiency for the sake of the analysis. In actuality, this efficiency can differ according to factors such as speed, load, lubrication, and so on.
2. It is thought that gear mesh losses have dominant impacts on the overall performance of the gear system. There are uncounted-power losses like bearing losses, wind age losses, etc.
3. The overall efficiency of the drivetrain would depend on other parts that aren't taken into account, such as motors and power electronics.

9. Conclusions

A systematic approach for studying and calculating the efficiency and power loss of PGTs is proposed. Initially, the nomograph of a two-input PGT is explained, from which the relative angular speeds of all components are easily derived. The speed sequence and operating conditions are then used to examine the torque and power of each link, which is used to analyze the power flow. On the nomograph, the distributions of input and output links are plotted to calculate the speed ratios between each link. Following that, the total efficiency is calculated using the friction losses of the two-input PGTs. A straightforward algorithm has been suggested to determine the route of power flow and confirm whether power circulation is present or not.The main conclusions that can be obtained are:

1. A methodical approach is suggested to determine the power losses and efficiency of a dual-input planetary gear mechanism while accounting for friction losses. This makes it possible to examine how power circulation affects system efficiency.
2. A dual-input planetary gear system can be studied in more depth if all of its operating modes are looked at.
3. This study will provide engineers a systematic approach for determining power flow paths, verifying power circulation, and evaluating the performance of PGTs in integrated wheel hub motors.
4. For the wheel hub motor's planetary gear arrangement, a larger gear ratio improves performance by lowering power losses and increasing overall efficiency. When the gear ratios are $Z_1/Z_4 = 4$, $Z_3/Z_2 = -1$, and $Z_2/Z_4 = 1$, the local efficiencies are 0.9, and the input velocity ratio β is 0.5, the total efficiency is greater than 93%, which exceeds the assumed local efficiencies of 0.9.
5. After identifying the conditions for no power circulation, an alternate configuration is offered that does not require power circulation.
6. Understanding the power flow through multi-path PGTs associated with the in-wheel motor transmission enables designers to make more informed decisions regarding the configuration that is or will be used.

Authors' contribution

All authors contributed equally to the preparation of this article.

Declaration of competing interest

The authors declare no conflicts of interest.

Funding source

This study didn't receive any specific funds.

Data availability

The data that support the findings of this study are available from the corresponding author upon reasonable request.

Acknowledgements

The authors would like to acknowledge.

REFERENCES

[1] H. Kwon, Y. Choi, W. Choi, and S. Lee, "Multimode dual-motor electric vehicle system for eco and dynamic driving," *Results in Engineering*, vol. 19, p. 101298, 2023. [Online]. Available: https://doi.org/10.1016/j.rineng.2023.101298

[2] F. Alanazi, "Electric vehicles: Benefits, challenges, and potential solutions for widespread adaptation," *Applied Sciences*, vol. 13, no. 10, 2023. [Online]. Available: https://doi.org/10.3390/app13106016

[3] Z. Wang, J. Zhou, and G. Rizzoni, "A review of architectures and control strategies of dual-motor coupling powertrain systems for battery electric vehicles," *Renewable and Sustainable Energy Reviews*, vol. 162, p. 112455, 2022. [Online]. Available: https://doi.org/10.1016/j.rser.2022.112455

[4] H. Liu, J. Zhao, T. Qing, X. Li, and Z. Wang, "Energy consumption analysis of a parallel phev with different configurations based on a typical driving cycle," *Energy Reports*, vol. 7, pp. 254–265, 2021. [Online]. Available: https://doi.org/10.1016/j.egyr.2020.12.036

[5] H. Kwon, Y. Choi, W. Choi, and S. Lee, "A novel architecture of multimode hybrid powertrains for fuel efficiency and sizing optimization," *IEEE Access*, vol. 10, pp. 2591–2601, 2022. [Online]. Available: https://doi.org10.1109/ACCESS.2021.3139029

[6] A. García and J. Monsalve-Serrano, "Analysis of a series hybrid vehicle concept that combines low temperature combustion and biofuels as power source," *Results in Engineering*, vol. 1, p. 100001, 2019. [Online]. Available: https://doi.org/10.1016/j.rineng.2019.01.001

[7] G. Mantriota and G. Reina, "Dual-motor planetary transmission to improve efficiency in electric vehicles," *Machines*, vol. 9, no. 3, 2021. [Online]. Available: https://doi.org/10.3390/machines9030058

[8] J. Wu, X. Hong, G. Feng, and Y. Zhang, "Seamless mode shift control for a new simpson planetary gearset based dual motor powertrain in electric vehicles," *Mechanism and Machine Theory*, vol. 178, p. 105056, 2022. [Online]. Available: https://doi.org/10.1016/j.mechmachtheory.2022.105056

[9] J. Wu, J. Liang, J. Ruan, N. Zhang, and P. Walker, "Efficiency comparison of electric vehicles powertrains with dual motor and single motor input," *Mechanism and Machine Theory*, vol. 128, pp. 569–585, 2018. [Online]. Available: http://hdl.handle.net/10453/131752

[10] T. Wu, F. Wang, and P. Ye, "Regenerative braking strategy of dual-motor ev considering energy recovery and brake stability," *World Electric Vehicle Journal*, vol. 14, no. 1, 2023. [Online]. Available: https://doi.org/10.3390/wevj14010019

[11] C. kai Wen, S. li Zhang, B. Xie, Z. he Song, T. hui Li, F. Jia, and J. gang Han, "Design and verification innovative approach of dual-motor power coupling drive systems for electric tractors," *Energy*, vol. 247, p. 123538, 2022. [Online]. Available: https://doi.org/10.1016/j.energy.2022.123538

[12] A. Hussein Juber, E. L. Esmail, and T. N. Ali, "Graph representation of planetary gear trains: A review," *Al-Qadisiyah Journal for Engineering Sciences*, vol. 14, no. 4, pp. 220–224, 2021. [Online]. Available: https://doi.org/10.30772/qjes.v14i4.893

[13] H. A. Nafeh and E. Lauibi Esmail, "Genetically compatible graphs for planetary gear train synthesis," *Al-Qadisiyah Journal for Engineering Sciences*, vol. 15, no. 1, pp. 9–17, 2022. [Online]. Available: https://doi.org/10.30772/qjes.v15i1.807

[14] X. Xu, J. Chen, Z. Lin, Y. Qiao, X. Chen, Y. Zhang, Y. Xu, and Y. Li, "Optimization design for the planetary gear train of an electric vehicle under uncertainties," *Actuators*, vol. 11, no. 2, 2022. [Online]. Available: https://doi.org/10.3390/act11020049

[15] X. Xu, J. Liang, Q. Hao, P. Dong, S. Wang, W. Guo, Y. Liu, Z. Lu, J. Geng, and B. Yan, "A novel electric dual motor transmission for heavy commercial vehicles," *Automotive Innovation*, vol. 4, no. 1, 2021. [Online]. Available: https://doi.org/10.1007/s42154-020-00129-7

[16] N.-T. Hoang and H.-S. Yan, "On the innovation design for two-motor transmissions with eight-link mechanisms in the electric vehicles," *Applied Sciences*, vol. 9, no. 1, 2019. [Online]. Available: https://doi.org/10.3390/app9010140

[17] NSK's Website. [Online]. Available: http://www.nsk.com/company/news/2017/press0119a.html

[18] K. Deepak, M. A. Frikha, Y. Benômar, M. El Baghdadi, and O. Hegazy, "In-wheel motor drive systems for electric vehicles: State of the art, challenges, and future trends," *Energies*, vol. 16, no. 7, 2023. [Online]. Available: https://doi.org/10.3390/en16073121

[19] X. Yang, Y. Shao, L. Wang, W. Yu, N. Yue, and W. Du, "Configuration design of dual-input compound power-split mechanism for in-wheel motor-driven electrical vehicles based on an improved lever analogy method," *Journal of Mechanical Design*, vol. 143, no. 10, p. 104501, 04 2021. [Online]. Available: https://doi.org/10.1115/1.4050653

[20] G. White, "Epicyclic gears from early hoists and winches—ii," *Mechanism and Machine Theory*, vol. 29, no. 2, pp. 309–325, 1994. [Online]. Available: https://doi.org/10.1016/0094-114X(94)90038-8

[21] B.-S. Kim, J.-J. Park, and J.-B. Song, "Double actuator unit with planetary gear train for a safe manipulator," *Proceedings 2007 IEEE International Conference on Robotics and Automation*, pp. 1146–1151, 2007. [Online]. Available: https://doi.org/10.1109/ROBOT.2007.363139

[22] D. Rabindran and D. Tesar, "Power flow analysis in parallel force/velocity actuators (pfva): Theory and simulations," *Volume 2: 32nd Mechanisms and Robotics Conference, Parts A and B*, pp. 983–992, 08 2008. [Online]. Available: https://doi.org/10.1115/DETC2008-49164

[23] F. Zhu, L. Chen, and C. Yin, "Scheme design and optimal selection for hev planetary gear coupling mechanism," *Volume 6: ASME Power Transmission and Gearing Conference; 3rd International Conference on Micro- and Nanosystems; 11th International Conference on Advanced Vehicle and Tire Technologies*, pp. 943–949, 08 2009. [Online]. Available: https://doi.org/10.1115/DETC2009-86716

[24] K.-B. Sheu, "Analysis and evaluation of hybrid scooter transmission systems," *Applied Energy*, vol. 84, no. 12, pp. 1289–1304, 2007. [Online]. Available: https://doi.org/10.1016/j.apenergy.2006.10.004

[25] J. Kim, N. Kim, S. Hwang, Y. Hori, and H. Kim, "Motor control of input-split hybrid electric vehicles," *International Journal of Automotive Technology*, vol. 10, p. 733–742, 2009. [Online]. Available: https://doi.org/10.1007/s12239-009-0086-1

[26] F. Zhang, H. Liu, Y. Hu, and J. Xi, "A supervisory control algorithm of hybrid electric vehicle based on adaptive equivalent consumption minimization strategy with fuzzy pi," *Energies*, vol. 9, no. 11, 2016. [Online]. Available: https://doi.org/10.3390/en9110919

[27] H. A. Hussen, E. L. Esmail, and R. A. Hussen, "Power flow simulation for two-degree-of-freedom planetary gear transmissions with experimental validation," *Modelling and Simulation in Engineering*, vol. 2020, no. 1, p. 8837605, 2020. [Online]. Available: https://doi.org/10.1155/2020/8837605

[28] X. Zhao and P. Maißer, "A novel power splitting drive train for variable speed wind power generators," *Renewable Energy*, vol. 28, no. 13, pp. 2001–2011, 2003. [Online]. Available: https://doi.org/10.1016/S0960-1481(03)00127-7

[29] E. L. Esmail, "Nomographs for synthesis of epicyclic-type automatic transmissions," *Meccanica*, vol. 48, p. 2037–2049, 2013. [Online]. Available: https://doi.org/10.1016/S0960-1481(03)00127-7

[30] E. L. Essam, "Influence of the operating conditions of two-degree-of-freedom planetary gear trains on tooth friction losses," *Journal of Mechanical Design*, vol. 140, no. 5, p. 054501, 03 2018. [Online]. Available: https://doi.org/10.1115/1.4039452

How to cite this article:
Gaidaa Shaker Kareem and Essam L. Esmail. (2025). 'Circulating power analysis in dual-input planetary gear mechanisms employed in in-wheel motor-driven electrical vehicles', Al-Qadisiyah Journal for Engineering Sciences, 18(2), pp. 211-221. https://doi.org/10.30772/qjes.2024.146323.1102